ELSEVIER

Cardiovascular Research 59 (2003) 67–77

Cardiovascular Research

www.elsevier.com/locate/cardiores

Depletion of T-tubules and specific subcellular changes in sarcolemmal proteins in tachycardia-induced heart failure

Ravi C. Balijepalli[a], Andrew J. Lokuta[b], Nathan A. Maertz[b], Jennifer M. Buck[a], Robert A. Haworth[c], Hector H. Valdivia[b], Timothy J. Kamp[a,b,*]

[a]*Department of Medicine, University of Wisconsin, Madison, WI, USA*
[b]*Department of Physiology, University of Wisconsin, Madison, WI, USA*
[c]*Department of Surgery, University of Wisconsin, Madison, WI, USA*

Received 7 November 2002; accepted 18 February 2003

Abstract

Objective: The T-tubule membrane network is integrally involved in excitation–contraction coupling in ventricular myocytes. Ventricular myocytes from canine hearts with tachycardia-induced dilated cardiomyopathy exhibit a decrease in accessible T-tubules to the membrane-impermeant dye, di8-ANNEPs. The present study investigated the mechanism of loss of T-tubule staining and examined for changes in the subcellular distribution of membrane proteins essential for excitation–contraction coupling. **Methods:** Isolated ventricular myocytes from canine hearts with and without tachycardia-induced heart failure were studied using fluorescence confocal microscopy and membrane fractionation techniques using a variety of markers specific for sarcolemmal and sarcoplasmic reticulum proteins. **Results:** Probes for surface glycoproteins, Na/K ATPase, Na/Ca exchanger and $Ca_v1.2$ demonstrated a prominent but heterogeneous reduction in T-tubule labeling in both intact and permeabilised failing myocytes, indicating a true depletion of T-tubules and associated membrane proteins. Membrane fractionation studies showed reductions in L-type Ca^{2+} channels and β-adrenergic receptors but increased levels of Na/Ca exchanger protein in both surface sarcolemma and T-tubular sarcolemma-enriched fractions; however, the membrane fraction enriched in junctional complexes of sarcolemma and junctional sarcoplasmic reticulum demonstrated no significant changes in the density of any sarcolemmal protein or sarcoplasmic reticulum protein assayed. **Conclusion:** Failing canine ventricular myocytes exhibit prominent depletion of T-tubules and changes in the density of a variety of proteins in both surface and T-tubular sarcolemma but with preservation of the protein composition of junctional complexes. This subcellular remodeling contributes to abnormal excitation–contraction coupling in heart failure.

Keywords: Ca-channel; E-c coupling; Heart failure; Remodeling; Sarcolemma

1. Introduction

In adult mammalian ventricular myocytes, the transverse tubule (T-tubule) network represents a complex system of interconnected membrane structures continuous with the extracellular space. This membrane network provides up to 50–60% of the surface area of the myocyte and is integrally involved in multiple cellular processes including membrane transport, excitability, cellular signaling, and excitation–contraction (EC) coupling [1,2]. T-tubules are also the site of most junctional complexes formed between sarcolemma containing L-type Ca^{2+} channels and junctional sarcoplasmic reticulum with Ca^{2+} release channels or ryanodine receptors (RyR). Thus, the initiation of EC coupling in ventricular myocytes is highly localized to the T-tubule network [3]. However, in disease states the T-tubule network can be dramatically altered [4–7]. In the canine tachycardia-induced dilated cardiomyopathy model, we have previously demonstrated remodeling of isolated

*Corresponding author. H6/343 Clinical Science Center, Box 3248, 600 Highland Ave., Madison, WI 53792, USA. Tel.: +1-608-263-4856; fax: +1-608-263-0405.
E-mail address: tjk@medicine.wisc.edu (T.J. Kamp).

Time for primary review 24 days.

0008-6363/03/$ – see front matter
doi:10.1016/S0008-6363(03)00325-0

ventricular myocytes characterized by a prominent reduction in the density of T-tubule staining by the membrane impermeant dye, Di-8-ANNEPs, and an increase in cell size mostly due to an increase in myocyte length [7].

The basis for the loss of T-tubule staining by the membrane impermeant di-8-ANNEPs in failing ventricular myocytes is unknown. At least two distinct possibilities underlie this observation. First, T-tubules may simply seal off from the surface membrane and remain sealed intracellular membrane structures. Alternatively, T-tubules could be truly depleted from the failing cells with loss of these membranes and associated proteins. To discriminate between these possibilities as well as verify the di-8-ANNEPs results, we used fluorescence confocal microscopy to examine a variety of sarcolemmal membrane proteins including the α_{1C} subunit ($Ca_v1.2$) of the L-type Ca^{2+} channel, surface membrane glycoproteins recognized by the lectin wheat germ agglutinin (WGA), the Na/Ca exchanger (NCX), and the Na/K ATPase. Labeling of both intact, living myocytes and permeabilised cells was performed to allow detection of T-tubules contiguous with the surface sarcolemma as well as internalized T-tubules. We observed a heterogeneous loss of T-tubule staining for all membrane proteins similar to the previous findings with di-8-ANNEPs.

The prominent loss of T-tubules suggested that the protein composition of the sarcolemmal and junctional sarcoplasmic reticulum membranes may be fundamentally altered in the failing myocytes. Changes in membrane proteins cannot be easily quantified by fluorescence microscopy, and so we utilized membrane fractionation techniques and measured the abundance of critical proteins involved in EC coupling. Membranes enriched in surface sarcolemma, T-tubule sarcolemma and junctional complexes of sarcolemma with junctional sarcoplasmic reticulum were prepared [8]. We found distinctive changes in membrane proteins in both surface sarcolemma and T-tubular sarcolemmal fractions but not in the fraction enriched in junctional complexes. No changes were observed for sarcoplasmic reticulum proteins. Overall, these findings demonstrate remarkable remodeling of the failing ventricular myocyte with a depletion of T-tubules and changes in the density of a number of essential proteins in the sarcolemma in the failing myocyte. A preliminary report of these results has been presented [9].

2. Methods

2.1. Pacing-induced heart failure and isolation of canine ventricular myocytes

The investigation conforms with the *Guide for the Care and Use of Laboratory Animals* published by the US National Institutes of Health (NIH Publication No. 85-23, revised 1996). Rapid ventricular pacing at 220–250 beats/min for 4–6 weeks was used to produce a dilated cardiomyopathy in mongrel dogs, and myocytes were enzymatically isolated as previously described [7]. A total of 15 sham-operated control dogs and 16 tachycardia-paced dogs were used in these studies. Heart failure was reproducibly present in tachycardia-paced dogs as confirmed by hemodynamic measurements at the time of killing (control vs. DCM: dP/dt_{max} 1520±405 vs. 680±123 mmHg/s; dP/dt_{min} −1193±347 vs. −790±273 mmHg/s; LVEDP 5.7±2.5 vs. 19±9.9 mmHg).

2.2. Fluorescence confocal microscopy

WGA coupled to Alexafluor-488 and BODIPY-Ouabain (used to visualize the Na, K-pump protein in the myocytes) were purchased from Molecular Probes (Eugene, OR). Living myocytes were incubated with 100 μg/ml WGA and 5 μM BODIPY-Ouabain for 30 min and 1 h, respectively, at room temperature, washed three times with Tyrode solution, then mounted on a coverslip for image acquisition [10].

Immunolabeling was performed on ventricular myocytes using a rabbit polyclonal antibody to the L-type Ca^{2+} channel α_{1C} subunit ($Ca_v1.2$, gift from Dr J. Hell) [11] and the mouse monoclonal antibody to the Na^+/Ca^{2+} exchanger (NCX, C2C12 antibody, Affinity Bioreagents, Inc., Golden, CO) as described previously [12]. Imaging was performed with a Bio-Rad MRC 1024 laser scanning confocal microscope. Randomly selected myocytes from control and failing animals were imaged in *Z*-axis in 1 μm steps and fluorescence signal was Kalman-averaged three times. Analysis of the cells and T-tubule area was performed with NIH Image 1.62 software. Cell area was estimated based on known pixel size and number of pixels within the cell image. T-tubule area was estimated by considering the subset image produced by those pixels that are inside the cell image, and pixels highlighting the perimeter were excluded. Pixels in this subset image were separated by a threshold into pixels of either high intensity or low intensity, with high intensity pixels represented by a different color. The ratio of T-tubule/cell area was estimated from the total number of pixels above the threshold and total number of pixels in the cell image. The T-Index for an individual cell was calculated by averaging the ratio of T-tubule area/cell area for each image in the *Z*-series. Thus, the T-index provides a semi quantitative index of the relative abundance of T-tubules in a myocytes.

2.3. Membrane fractionation

Sarcolemmal, T-tubular, and dyadic membrane fractions were prepared as previously described with slight modifications [8]. Briefly, 30–35 g of canine left ventricle was homogenised and subjected to a series of differential centrifugations. Homogenised, washed membranes largely

free of myofilament and soluble proteins, were saved as the crude membrane homogenate (H). Membrane material was loaded onto a continuous (10–40%) or a discontinuous sucrose density gradient of 21, 31, 40, and 55% sucrose. Continuous gradients were centrifuged overnight at 141,000×g_{max}, and discontinuous gradients were centrifuged for 2 h at 141,000×g_{max} resulting in three distinct interfaces at 10/21% sucrose (Fraction-I), 21/31% sucrose (Fraction-II), and 31/40% sucrose (Fraction-III). Protein concentration was determined by the Lowry method.

2.4. Na/K-ATPase activity

Ouabain (5 μM) inhibitable Na, K-ATPase activity in the membrane fractions was assayed in the presence of optimal concentrations of sodium dodecyl sulfate (F-I and F-II, 0.001%; and F-III, 0.005% SDS). Enzyme activity was assayed in a buffer containing (in mM) 50 Histidine, 100 NaCl, 6 KCl, 4 $MgCl_2$, 4.5 NaN_3, 1 EGTA, 3 ATP, 2.7 phosphoenol pyruvate, and 75 μg/ml pyruvate kinase.

2.5. Radioligand binding

Equilibrium (+)-[^{3}H]PN200-110, [^{125}I]-iodocyanopindolol and [^{3}H] ryanodine binding assays were conducted as previously described [8,13,14] using a vacuum filtration method with a 24-well harvester (Brandel, Gaithersburg, MD). All radioligand-binding assays were performed in triplicate, and a subset of the experiments did complete saturation binding curves for each ligand in each fraction. Data were fit to a single site-binding model by non-linear regression analysis using Origin 6.0 (Microcal, Northampton, MA).

2.6. Quantitative Western analysis

SDS–PAGE and Western blot analysis was carried out for Na/Ca exchanger (C2C12), SERCA2a, ryanodine receptor (RyR2) using specific antibodies (Affinity Bioreagents, Inc., Golden, CO), and calsequestrin (CSQ) (Research Diagnostics, Lexington, KY). Membrane proteins (60 μg) from each of the membrane fractions from control and failed dogs separated on 7.5% gels were transferred to nitrocellulose membrane for 1 h at 105 V. Immunoreaction was detected using a primary antibody to NCX (1:1000) and CSQ (1:2500) and using secondary antibodies goat anti-mouse IgG conjugated to HRP (1:20,000) for NCX, and donkey anti-rabbit IgG to HRP (1:50,000) for CSQ (Amersham Life Sciences, Cleveland, OH). Immunoreactivity was visualized using chemiluminescent detection system, ECL™ (Amersham Life Sciences, Cleveland, OH). For quantitation of immunoblots, linearity of the signal as a function of the amount of protein loaded (10–120 μg) was assured by establishing the relationship between antigen concentration and signal and by generating multiple exposures of autoradiograms. Western blot analysis of SERCA2a and RYR used 30 μg protein from each membrane fraction as described elsewhere [13].

2.7. French press treatment

The membrane material was passed through the French Pressure Cell (SLM-AMINCO, Rochester, NY) at 11,000 psi×2, with a flow rate adjusted to 2 ml/min. The resulting membranes and untreated membranes were layered onto a continuous gradient of 10–40% sucrose and centrifuged overnight at 141,000×g_{max}.

2.8. Statistics

Data are presented as mean±S.D. and significance was determined using a Student's *t*-test.

3. Results

3.1. Fluorescence confocal imaging of isolated cardiomyocytes

We examined the staining of intact, living myocytes with two surface membrane protein markers: WGA conjugated to Alexa-488, which recognizes sarcolemmal glycoproteins (Fig. 1A–C), and BODIPY-ouabain, which binds to the Na/K ATPase (Fig. 1D–F). Both of these fluorescent probes are membrane impermeant and are only accessible to surface sarcolemma and to intact T-tubule contiguous with the extracellular space. Confocal imaging of WGA labeled control myocytes revealed prominent staining of the surface sarcolemma forming the boundary of the cell as well as T-tubules throughout the cell (Fig. 1A). The T-tubules were recognized as an array of dots arranged in a linear fashion that result from the T-tubules viewed in cross-section [1,3,7]. In the failing myocytes a clear peripheral staining was observed indicating surface sarcolemmal staining; however, there was a clear loss of the regular array of WGA-stained T-tubules in all the failing cells studied (Fig. 1B,C). As reported previously with di-8-ANNEPs staining [7], the reduction in T-tubule staining was variable among cells studied from a given dog with some cells showing the prominent drop out only at the ends of the cells (Fig. 1B) while other cells showed more diffuse loss of T-tubule staining (Fig. 1C).

Likewise, imaging of myocytes stained with BODIPY-ouabain demonstrated a loss of T-tubule staining in failing myocytes (Fig. 1E,F) compared to the regular array of T-tubules seen in control (Fig. 1D). To quantify the extent of T-tubules present in the cells, we determine the T-index for each cell, which is the proportion of the total cell area stained for T-tubules averaged for the collection of images obtained in a *Z*-series (see Methods). Fig. 2 shows that the T-index for WGA labeling was significantly decreased in

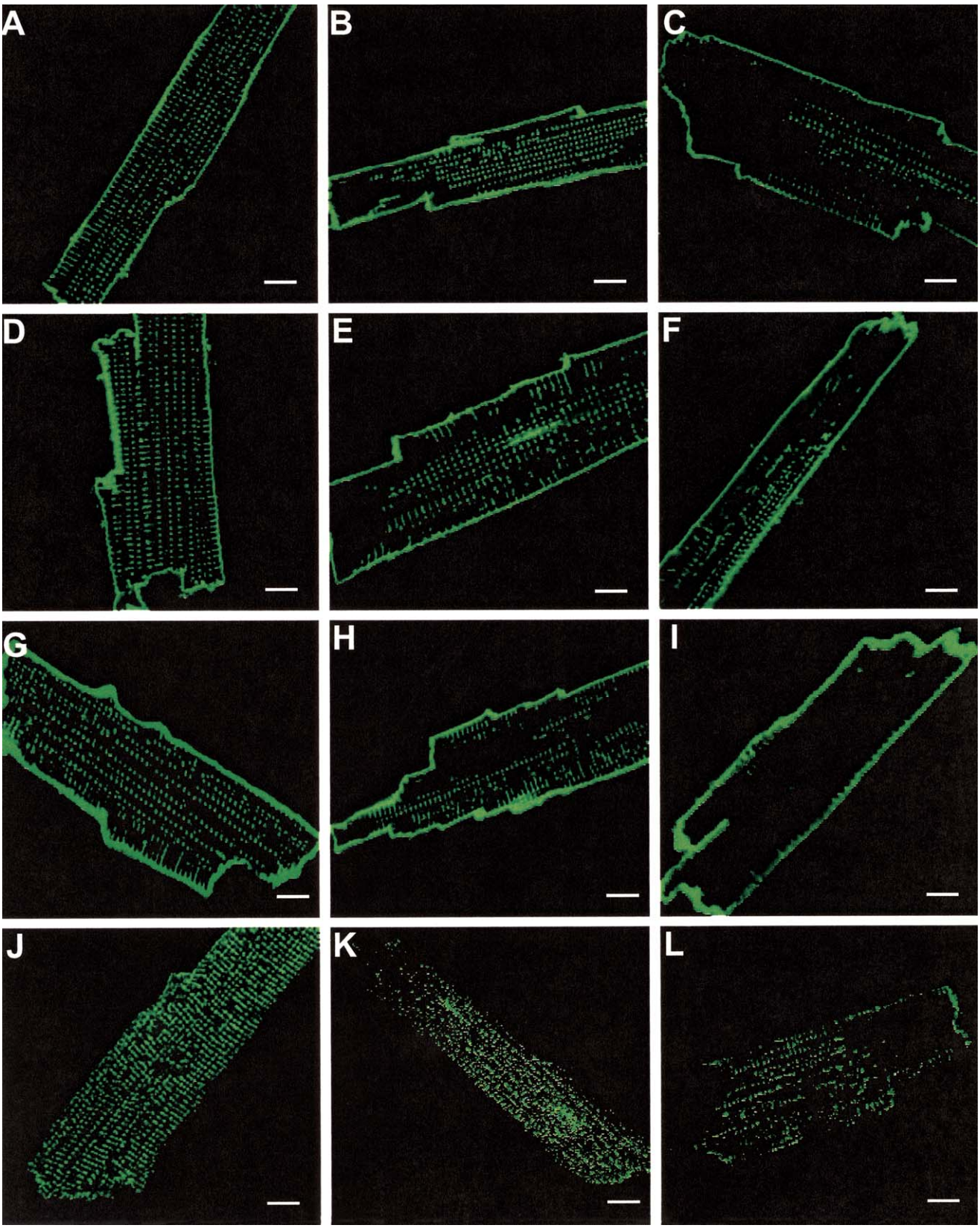

Fig. 1. Laser scanning confocal images of representative canine ventricular myocytes isolated from control (A,D,G,J—first column) and failing (B,C,E,F,H,I,K,L—second and third columns) hearts. Intact, living myocytes are shown in the first two rows stained with WGA-Alexa-488 (A–C) or BODIPY-ouabain (D–F). Fixed, permeabilised myocytes are shown in the last two rows immunostained using antibodies to NCX (G–I) and $Ca_v1.2$ (J–L). Scale bar is 5 μm.

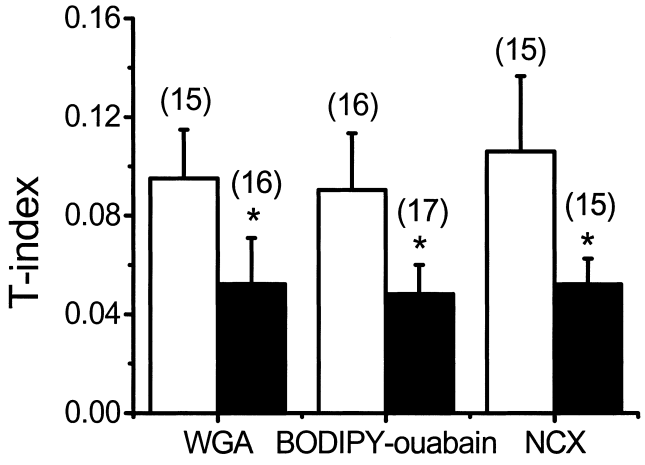

Fig. 2. Decreased T-index in the failing canine myocytes. The T-index was calculated for each cell stained with WGA, Bodipy-ouabain and NCX using the *Z*-series of images (see Methods), and the average T-index for control (open) and failing (filled) myocytes is plotted. Number in parenthesis indicates the number of cells/dogs analyzed. *$P<0.001$.

failing cells compared to control cells (5±2% vs. 10±2%, $P<0.001$). Likewise, the T-index was comparably decreased in failing cells for the BODIPY-oubain staining (Fig. 2).

For comparison, immunostaining experiments were then carried out on permeablized, fixed myocytes using antibodies directed against the Na/Ca exchanger (NCX) and the L-type Ca^{2+} channel α_{1C} subunit ($Ca_v1.2$). In control myocytes, the NCX immunostaining (Fig. 1G) was comparable to that observed for WGA-Alexa-488 and BODIPY-ouabain with prominent surface sarcolemmal as well as T-tubular staining. The antibody directed against $Ca_v1.2$ demonstrated a prominent T-tubule-staining pattern in control myocytes (Fig. 1J), but the staining of periphery of the cell at the surface sarcolemma was relatively faint. Failing myocytes immunostained for either NCX or $Ca_v1.2$ showed a variable loss of T-tubule staining (Fig. 1H,I,K,L). The T-index demonstrated that for permeabilised myocytes stained for the NCX protein that there was a decrease in T-tubules in failing cells compared to control (5±1% vs. 11±3%) similar to the decrease observed for WGA Alexa-488 and BODIPY-ouabain (Fig. 2). The T-index was not calculated for $Ca_v1.2$ immunostaining as the signal was less intense and surface sarcolemmal labeling was faint.

Together, these comparable results in intact and permeabilised myocytes demonstrate that failing canine myocytes have a true depletion of T-tubule structures and associated proteins. This prominent cellular remodeling is also associated with a change in dimension of the myocytes as average surface area was increased from 3393±344 μm^2 in control cells ($n=46$) to 4287±360 μm^2 in failing cells ($n=48$) consistent with cellular hypertrophy. Because cellular remodeling may also be associated with changes in the relative abundance of the sarcolemmal proteins and fluorescence determination of membrane protein density is not easily quantified, we next turned to biochemical assays using enriched sarcolemmal membrane preparations.

3.2. Membrane fractionation of canine ventricular myocardium

Sarcolemmal-enriched membranes from canine ventricular myocardium were prepared as described in Methods. Based on previous characterization of this membrane preparation from ovine and bovine heart [8], we examined the distributions in continuous sucrose gradients of three seminal membrane markers: sarcolemmal Na/K-pump measured by ouabain-sensitive ATPase activity, sarcolemmal L-type Ca^{2+} channels using (+)-[^{3}H]PN200-110 binding, and SR Ca^{2+} release channels using [^{3}H]ryanodine binding. The total (Fig. 3A) and normalized (Fig. 3B) activity for these three membrane markers for a representative sucrose gradient from a control canine heart are shown. The Na/K-ATPase activity was greatest in the lower density regions of the gradient with the peak activity at 21% sucrose indicating the greatest enrichment of surface sarcolemma in this region. In contrast, binding of

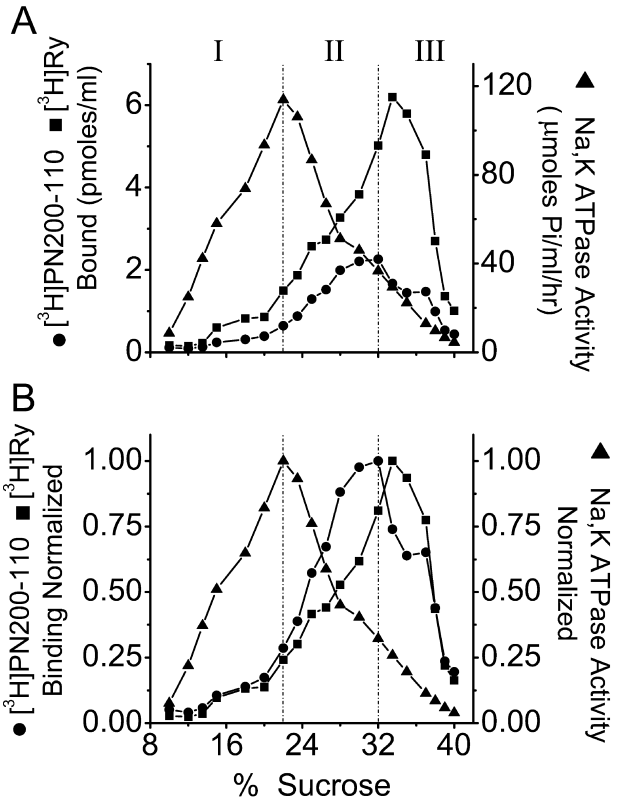

Fig. 3. Continuous sucrose density gradient separation of left ventricular membranes from a representative control dog assayed for ouabain-inhibitable Na/K-ATPase activity (▲), (+)-[^{3}H] PN 200-110 binding at 0.25 nM (●) and [^{3}H]ryanodine binding (■) at 0.1 nM. Panel A shows the total activity, and panel B displays the normalized data.

[^{3}H]ryanodine was most prominent in heavier fractions of the gradient with a peak in the binding at 35% sucrose demonstrating enrichment of junctional sarcoplasmic reticulum in the densest region of the gradient. The binding of (+)-[^{3}H]PN200-110 to L-type Ca^{2+} channels showed the most complex and broad distribution in the sucrose gradient. As best seen in Fig. 3B, there was evidence for three peaks of binding for (+)-[^{3}H]PN200-110 with a small peak in the low density region of the gradient in the range of the 15–22% sucrose overlapping the greatest Na/K ATPase activity. The second and greatest peak of total activity was in the middle range of the gradient peaking at 30–32% sucrose, and a distinct shoulder occurred in the densest region of the gradient. The very distinct distribution of the two sarcolemmal membrane markers, Na/K ATPase and L-type Ca^{2+} channels, provides evidence for at least two different components of sarcolemma present in the gradient, namely surface sarcolemma and T-tubular sarcolemma as suggested previously [8,15]. Furthermore, the presence of significant (+)-[^{3}H]PN 200-110 binding in the highest density region of the gradients together with the peak [^{3}H]ryanodine binding suggests the presence of intact junctional complexes in this region of the gradient. Based on these results and a previous study [8], the sarcolemmal membranes were then separated on discontinuous sucrose gradients into three major fractions: surface sarcolemma-enriched (F-I, 21% sucrose); T-tubular sarcolemma-enriched (F-II, 21–31% sucrose), and sarcolemma in junctional complexes with SR (F-III, 31–40% sucrose).

3.3. Changes in density of sarcolemma proteins in canine heart failure

Membranes were prepared from control (n=7) and failing (n=7) canine ventricles, then separated on a discontinuous sucrose gradient. Total protein and four specific sarcolemmal proteins important in EC coupling were assayed in the three fractions and a membrane homogenate as shown in Fig. 4. The F-II fraction had the greatest amount of total protein recovered from the gradient, but there was a significant 24% decrease in F-II protein in failing compared to control hearts. As F-II is the most enriched in T-tubular membranes, this finding is consistent with a decrease in the abundance T-tubules detected in the fluorescence imaging studies (see Figs. 1 and 2). The total membrane protein yield was similar in F-I and F-III.

The Na/K ATPase specific activity was greatest in F-I with a 10-fold enrichment relative to homogenate (Fig. 4B). Additionally, the Na/K ATPase activity was not significantly different comparing control and failing hearts in any of the three fractions or homogenate (Fig. 4B).

Binding of (+)-[^{3}H]PN200-110 to L-type Ca^{2+} channels showed a distinct distribution in the step gradient and was enriched in all three fractions relative to homogenate. The greatest specific binding was in F-II, consistent with the prominent T-tubular immunostaining of $Ca_v1.2$. In membranes from failing hearts, binding sites for (+)-[^{3}H]PN200-110 were reduced by 46% and 31% compared to control for F-I and F-II, respectively (Fig. 4C), but in F-III there was no significant change in the number of binding sites. The affinity of binding (K_D) was comparable in all three fractions and unchanged in heart failure (Table 1).

The binding of the non-selective β-adrenergic receptor antagonist, [^{125}I]-CYP was distributed in the three fractions of the gradient similar to Na/K ATPase activity with the highest binding site density present in F-I (Fig. 4D). Failing left ventricular membranes showed a significant 29% decrease in the number of [^{125}I]-CYP binding sites from both F-I and F-II, but there was no significant change in F-III. The affinity (K_D) was not appreciably different in all fractions and unchanged in heart failure (Table 1).

Quantitative Western blot analysis detected a single band at 120 kDa for NCX protein for both control and failing dog membrane fractions (Fig. 4E). The distribution of the NCX protein in different membrane fractions was similar to the distribution of β-ARs and Na/K ATPase activity with the greatest density in F-I (Fig. 4F). In heart failure, the exchanger protein was increased to 166±17% and 162±35% in F-I and F-II fractions, respectively.

3.4. Unchanged SR proteins in heart failure

The preparation also contains membranes derived from the sarcoplasmic reticulum. The SR is composed of longitudinal, corbular, and junctional components [16]. First we assessed the amount of the Ca^{2+} ATPase, SERCA2a, which is known to be present in all components of the SR. Fig. 5A shows that signal for SERCA2a was present in all membrane fractions, and there were no significant differences between membranes obtained from control hearts and failing hearts in any of the fractions or in homogenate. The SERCA2a Western blot signal was similar in the three membrane fractions showing a two to threefold enrichment from homogenate.

Binding of [^{3}H]ryanodine to the Ca^{2+} release channel present in the junctional and corbular SR was measured in all fractions. No significant differences were observed in the density of binding sites between failing and control samples in all three fractions and the homogenate. The affinity of [^{3}H]ryanodine was also unchanged (inset Fig. 5B and Table 1). Interestingly, the greatest density of [^{3}H]ryanodine binding sites was in F-II, whereas we predicted that F-III would contain more junctional SR-based on the previous study of Doyle et al. [8], which measured a 3.5-fold greater ryanodine-sensitive [$^{45}Ca^{2+}$] uptake in F-III than F-II. We hypothesized that these observations could be the result of small junctional SR

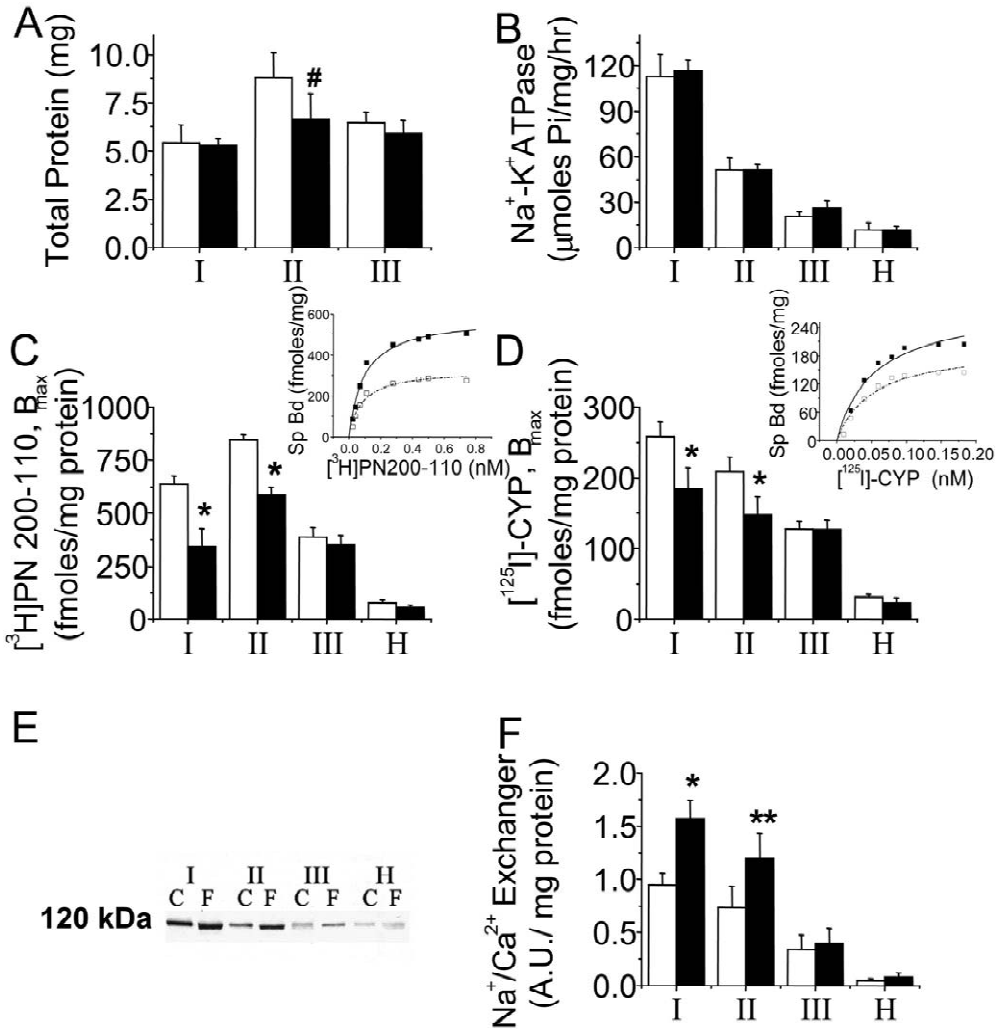

Fig. 4. Comparison of sarcolemmal membrane protein densities from discontinuous sucrose density gradient membrane fractions prepared from control (open bars) and failing (filled bars) canine left ventricles. Membrane fractions at 10/21% sucrose interface (F-I), 21/31% sucrose interface (F-II), 31/40% sucrose interface (F-III) and homogenate (H) were assayed for total protein (panel A), Na/K-ATPase activity (panel B), (+)-[^{3}H] PN 200-110 B_{max} (panel C), [^{125}I]-CYP B_{max} (panel D) and NCX protein (panels E,F). Insets in panels C and D show representative equilibrium binding curves for control (■) and failing (□) membranes from F-II. Panel E shows representative Western blot analysis using C2C12 antibody directed against the NCX protein. Data (mean±S.D.) are from seven control and seven failing dogs, #$P<0.01$; *$P<0.001$; **$P<0.005$.

Table 1
Measured affinity constants (KD) for (+)-[^{3}H]PN200-110, [^{3}H]ryanodine and [^{125}I]-CYP equilibrium binding to control (C) and failing (F) left ventricular membrane fractions F-I, F-II and F-III

	F-I		F-II		F-III	
	C	F	C	F	C	F
(+)-[^{3}H]-PN200-110 K_D (nM) (n=3)	0.134±0.019	0.116±0.014	0.144±0.027	0.115±0.014	0.118±0.017	0.125±0.017
[^{125}I]-CYP K_D (nM) (n=3)	0.058±0.016	0.056±0.02	0.069±0.015	0.074±0.017	0.050±0.009	0.063±0.012
[^{3}H]-ryanodine K_D (nM) (n=1)	0.75	1.50	1.00	1.50	1.00	1.20

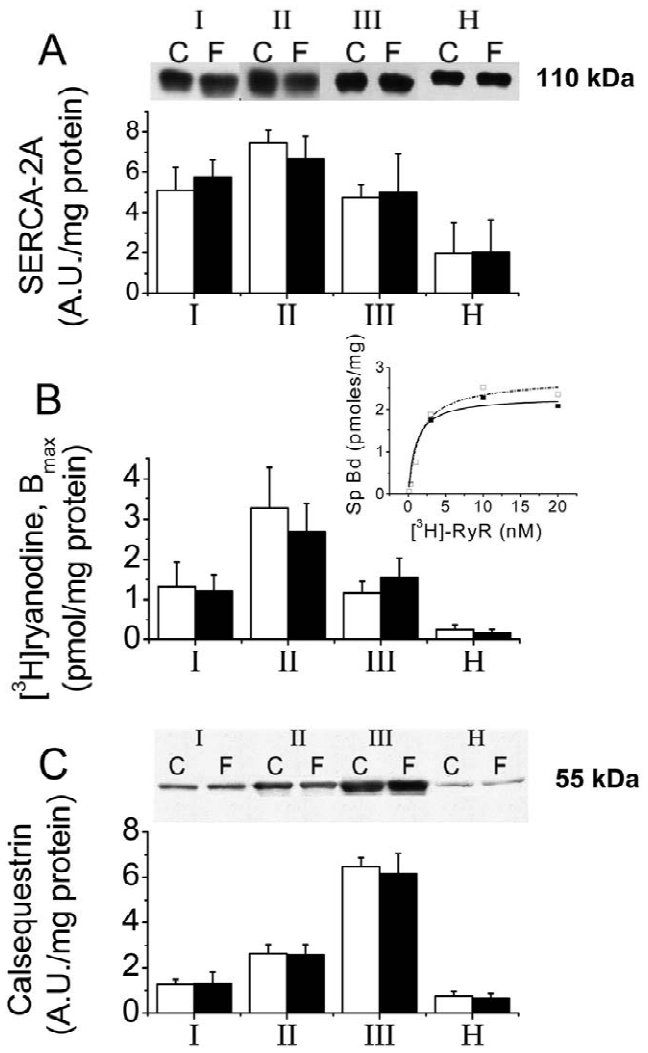

Fig. 5. Comparison of SR proteins from discontinuous sucrose density gradient membrane fractions prepared from control (open bars) and failing (filled bars) canine left ventricles. Panel A shows a representative Western blot for SERCA2a and average data (mean±S.D.) obtained from densitometry. Panel B shows the average B_{max} [^{3}H]ryanodine binding with the insert showing saturation binding curves of F-II from control (●) and failing (○). Panel C shows a representative Western blot for calsequestrin and average data obtained from densitometry.

fragments being present in F-II rather than intact junctional SR vesicles, which are enriched in F-III.

To further define the presence of junctional SR in this membrane preparation, we used immunoblots to determine the abundance of calsequestrin, which is highly enriched in junctional and corbular SR [17]. Calsequestrin is a critical Ca^{2+} binding protein present in the SR lumen, which helps buffer the high Ca^{2+} load. We predicted that this protein would be most enriched in F-III based on the assumption that there are intact junctional SR vesicles present in this fraction with the trapped calsequestrin and the ability to take up [$^{45}Ca^{2+}$]. Fig. 5C demonstrates the greatest enrichment in calsequestrin in F-III, and furthermore, there was no significant change in calsequestrin in control and failing samples.

3.5. French press study of junctional complexes

To test the hypothesis that intact junctional complexes were present specifically in F-III, we used the French press technique, which utilizes high pressure to separate membranes, essentially unzipping junctional complexes. The F-III fraction from a control dog was passed through French press, and resulting material was separated on continuous sucrose gradient (10–40%). Representative binding curves of (+)-[^{3}H]PN200-110 and [^{3}H]ryanodine from F-III with and without French press treatment are presented in Fig. 6. These data are representative of three independent experiments using different dog membrane preparations. Without French press treatment, binding for both markers was greatest in the range of 28–38% of

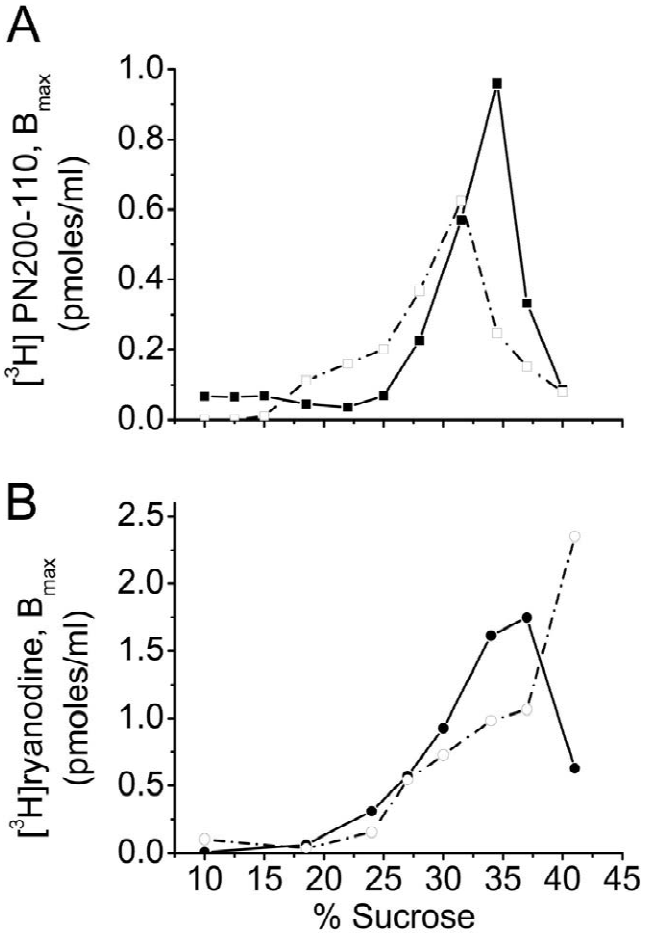

Fig. 6. Continuous sucrose density gradient (10–42%) separation of canine F-III membranes treated with and without French press and assayed for [^{3}H] PN 200-110 and [^{3}H]ryanodine binding. Panel A shows that [^{3}H] PN 200-110 binding sites were shifted to lower densities on the gradient with French press treatment (□) than without (■). Panel B demonstrates the opposite pattern for [^{3}H]ryanodine binding with a shift to higher density regions with French press (○) than without (●).

sucrose with binding for both peaking at 34% sucrose. French press treatment resulted in shifting the (+)-[^{3}H]PN200-110 binding sites to lower sucrose density regions of the gradient with the peak binding at 30% sucrose (Fig. 6A), whereas the [^{3}H]ryanodine binding sites shifted to the higher sucrose density regions with the peak at 40% sucrose (Fig. 6B). These results are consistent with separation by the French press of the two membrane components of the junctional complexes (sarcolemma and junctional SR), which then migrate to their distinct buoyant densities in the sucrose gradient. In F-I and F-II, French press treatment did not show any such changes in the (+)-[^{3}H]PN200-110 and [^{3}H]ryanodine peak binding on the continuous sucrose gradient (data not shown).

4. Discussion

4.1. Depletion of T-tubules in heart failure

Surprisingly few studies have examined the T-tubule system in cardiac disease. Early studies documented that during compensated hypertrophy, the T-tubule system rapidly increases in amount and allows the cell to maintain a constant surface area to volume ratio [18,19]. In addition, the relative ratio of surface area to cell volume is species-dependent, and for a given species the ratio is remarkably constant [20]. However, as compensated hypertrophy transitions to heart failure, an earlier electron microscopy study of SHR rats showed a decline in the volume fraction of T-tubules after an initial compensatory increase [19]. Our previous study in the canine tachycardia-induced heart failure model revealed a loss of T-tubule staining by the membrane impermeant di-8-ANNEPs in failing myocytes [7], and the present study demonstrates that this loss of staining is due to depletion of T-tubules and not simple internalization of the membranes. The extent of this depletion varies from cell to cell from a given dog but was evident in each cell imaged. How broadly this finding extends to other models of heart failure and human heart failure is unknown. In a doxorubicin cardiomyopathy model, a relative decrease in T-tubule density was suggested on the basis of unchanged cell size but decreased whole-cell capacitance [5]. Electron microscopy studies of human cardiomyopathic tissue have suggested both a proliferation of aberrantly shaped T-tubules [4] as well as a relative loss of T-tubules [21].

4.2. Changes in density of sarcolemmal and SR proteins

Both decreases (L-type Ca^{2+} channels and βAR) and increases (NCX) in the density of critical sarcolemmal membrane proteins were found in failing myocardium largely in agreement with previous studies [22–25]. The decrease in (+)-[^{3}H]-PN200-110 binding sites is in agreement with our previous charge movement study in this model of heart failure and studies in human failing ventricular myocytes suggesting a decrease in the density of L-type Ca^{2+} channels [7,26,27]. The novel data presented here are that these changes in sarcolemmal protein density occur similarly in both surface (F-I) and T-tubular sarcolemmal fractions (F-II) but not in F-III. Previous studies have not been able to directly address this important localization issue.

Measurements of SR-associated proteins including SERCA-2a, RyR, and calsequestrin failed to show significant changes in any of the fractions. Our finding of no change in SERCA-2a levels contrasts to a previous study in the same canine model that showed a 28% decrease [24]. The reason for this difference is unclear, but it is notable that previous studies in human heart failure have shown conflicting results with either a decrease or no change in SERCA-2a levels in heart failure [25]. For the RyR, previous studies in the canine tachycardia model measured reduced numbers of RyRs [28,29]. In human heart failure, radioligand binding and measurement of protein levels with Western blots have shown a variety of results from decreased to increased RyR number, but most commonly no change [25]. Finally, in agreement with the literature, calsequestrin protein abundance was unchanged comparing control with failing samples [25].

4.3. Junctional domain protein composition preserved

The results of this study and previous studies demonstrate that F-III is enriched in intact junctional complexes composed of sarcolemma tightly zippered to junctional SR. The following findings support this conclusion: the greatest amount of SR luminal protein calsequestrin in F-III (Fig. 5c), the previous demonstration of the greatest ryanodine-sensitive Ca^{2+} uptake in this fraction [8], the previous electron microscopic evidence of intact junctions [8], and the French press separation of the SR and sarcolemma markers in F-III (Fig. 6). This means that intact, sealed junctional SR vesicles are present in F-III, which have preserved coupling to surface or T-tubular sarcolemma. Therefore, this preparation gives a unique ability to quantitatively examine the composition of the junctional complexes of F-III, which is not afforded by immunochemistry or biophysical means. Despite finding significant changes in a number of sarcolemmal proteins in F-I and F-II in heart failure, we found no change in the density of these proteins in F-III. This, coupled with the lack of change in several SR proteins, suggested that at the level of resolution of these biochemical studies, no remarkable change in the protein composition of the junctional domains occurs in this heart failure model.

4.4. Limitations

Membrane fractionation of ventricular myocardium is

inherently limited by the presence of multiple cell types in the myocardium including myocytes, endothelial cells, fibroblasts, and vascular smooth muscle cells. To determine if contaminating cell types would alter our conclusions, we fractionated isolated ventricular myocytes on identical discontinuous sucrose density gradients. A comparable distribution of the membrane markers utilized in this study was obtained for both isolated myocytes and intact myocardium (data not shown).

A second limitation of the present study is that it focuses on a single dilated cardiomyopathy model produced by tachycardia pacing in dogs. This model displays many features common to dilated cardiomyopathies including biventricular remodeling with chamber dilatation, significant reduction in ejection fraction, and time-dependent changes in neurohormonal levels. However, unlike many causes of heart failure, it evolves quickly with pacing, is not associated with significant hypertrophy, and is readily reversible. Therefore, whether similar cellular remodeling and T-tubule depletion occurs in other forms of heart failure requires additional research.

4.5. The failing myocyte phenotype

In summary, failing ventricular myocytes exhibit a depletion of T-tubules and have associated decreases in the density of L-type Ca^{2+} channels and β-adrenergic receptors in both surface and T-tubular sarcolemma. In contrast, the density of NCX protein is increased in both of these membrane domains. Functional studies by others have commonly implicated a greater role of the Ca transient on Na/Ca exchange and decreased SR load in failing myocytes [30–32]. All of these findings have remarkable resemblance to the fetal or neonatal mammalian myocytes where T-tubules are sparse and EC coupling is less dependent on SR Ca release than Na/Ca exchange [33]. Furthermore, the initiation of the Ca transient in fetal ventricular myocytes is spatially asynchronous propagating from the edge of the cell into the cell due to the absence of T-tubules. Thus, we predict that a major functional effect of depletion of T-tubules despite preserved protein composition of junctional domains will be a spatially asynchronous Ca transient, which will blunt the maximal activation of the myofilaments and on the whole organ level blunt dP/dt_{max} [34]. The heterogeneous nature of the loss of T-tubules from cell to cell may also impair contractile efficiency, as cells will show variable time courses of contractile activation. In addition, the heterogeneous depletion of T-tubules may lead to microheterogeneities in conduction and repolarization in the ventricle and thus contribute to the increased propensity for lethal ventricular arrhythmias in heart failure. Future research will be needed to determine the functional impact of T-tubule depletion on the mechanical and electrical properties of the failing heart.

Acknowledgements

This study was supported by NIH grants R01 HL61537; R01 HL61534; P01 HL47053. The authors gratefully acknowledge the technical support of Larry F. Whitesell for producing the canine tachycardia heart failure model, Medtronic Corporation for donating the pacemakers, Ed B. Maryon (Department of Genetics) for providing the French Press, and Laketa Entzminger for assistance with data analysis.

References

[1] Soeller C, Cannell MB. Examination of the transverse tubular system in living cardiac rat myocytes by 2-photon microscopy and digital image-processing techniques. Circ Res 1999;84:266–275.
[2] Amsellem J, Delorme R, Souchier C, Ojeda C. Transverse-axial tubular system in guinea pig ventricular cardiomyocyte: 3D reconstruction, quantification and its possible role in K^+ accumulation-depletion phenomenon in single cells. Biol Cell 1995;85:43–54.
[3] Shacklock PS, Wier WG, Balke CW. Local Ca^{2+} transients (Ca^{2+} sparks) originate at transverse tubules in rat heart cells. J Physiol 1995;487:601–608.
[4] Schaper J, Froede R, Hein S et al. Impairment of the myocardial ultrastructure and changes of the cytoskeleton in dilated cardiomyopathy. Circulation 1991;83:504–514.
[5] Keung EC, Toll L, Ellis M, Jensen RA. L-type cardiac calcium channels in doxorubicin cardiomyopathy in rats morphological, biochemical, and functional correlations. J Clin Invest 1991;87:2108–2113.
[6] Kawamura K, Kashii C, Imamura K. Ultrastructural changes in hypertrophied myocardium of spontaneously hypertensive rats. Jap Circ J 1976;40:1119–1145.
[7] He J, Conklin MW, Foell JD et al. Reduction in density of transverse tubules and L-type Ca^{2+} channels in canine tachycardia-induced heart failure. Cardiovasc Res 2001;49:298–307.
[8] Doyle DD, Kamp TJ, Palfrey HC, Miller RJ, Page E. Separation of cardiac plasmalemma into cell surface and T-tubular components. Distribution of saxitoxin- and nitrendipine-binding sites. J Biol Chem 1986;261:6556–6563.
[9] Balijepalli RC, Lokuta AJ, Maertz NA et al. Decreased density of L-type calcium channels in surface and T-tubular sarcolemma in heart failure. Biophys J 2002;82:1198.
[10] Stegemann M, Meyer R, Haas HG, Robert-Nicoud M. The cell surface of isolated cardiac myocytes—a light microscope study with use of fluorochrome-coupled lectins. J Mol Cell Cardiol 1990;22:787–803.
[11] Davare MA, Horne MC, Hell JW. Protein phosphatase 2A is associated with class C L-type calcium channels (Cav1.2) and antagonizes channel phosphorylation by cAMP-dependent protein kinase. J Biol Chem 2000;275:39710–39717.
[12] Scriven DR, Dan P, Moore ED. Distribution of proteins implicated in excitation-contraction coupling in rat ventricular myocytes. Biophys J 2000;79:2682–2691.
[13] Lokuta AJ, Rogers TB, Lederer WJ, Valdivia HH. Modulation of cardiac ryanodine receptors by a phosphorylation–dephosphorylation mechanism. J Physiol 1995;487:609–622.
[14] Bristow MR, Ginsburg R, Umans V et al. Beta 1- and beta 2-adrenergic-receptor subpopulations in nonfailing and failing human ventricular myocardium: coupling of both receptor subtypes to muscle contraction and selective beta 1-receptor down-regulation in heart failure. Circ Res 1986;59:297–309.

[15] Wibo M, Bravo G, Godfraind T. Postnatal maturation of excitation-contraction coupling in rat ventricle in relation to the subcellular localization and surface density of 1,4-dihydropryidine and ryanodine receptors. Circ Res 1991;68:662–673.
[16] Carl SL, Felix K, Caswell AH et al. Immunolocalization of sarcolemmal dihydropyridine receptor and sarcoplasmic reticular triadin and ryanodine receptor in rabbit ventricle and atrium. J Cell Biol 1995;129:673–682.
[17] Jorgensen AO, Campbell KP. Evidence for the presence of calsequestrin in two structurally different regions of myocardial sarcoplasmic-reticulum. J Cell Biol 1984;98:1597–1602.
[18] Anversa P, Olivetti G, Melissari M, Loud AV. Stereological measurement of cellular and subcellular hypertrophy and hyperplasia in the papillary muscle of adult rat. J Mol Cell Cardiol 1980;12:781–795.
[19] Page E, McCallister LP. Quantitative electron microscopic description of heart muscle cells. Application to normal, hypertrophied and thyroxin-stimulated hearts. Am J Cardiol 1973;31:172–181.
[20] Satoh H, Delbridge LMD, Blatter LA, Bers DM. Surface:volume relationship in cardiac myocytes studied with confocal microscopy and membrane capacitance measurements: Species-dependence and developmental effects. Biophys J 1996;70:1494–1504.
[21] Kostin S, Scholz D, Shimadi T et al. The internal and external protein scaffold of the T-tubular system in cardiomyocytes. Cell Tissue Res 1998;294:449–460.
[22] Mukherjee R, Spinale FG. L-type calcium channel abundance and function with cardiac hypertrophy and failure: A review. J Mol Cell Cardiol 1998;30:1899–1916.
[23] Brodde OE. β-Adrenergic receptors in failing human myocardium. Basic Res Cardiol 1996;91:35–40.
[24] O'Rourke B, Kass DA, Tomaselli GF, Kaab S, Tunin R, Marban E. Mechanisms of altered excitation-contraction coupling in canine tachycardia-induced heart failure. I. Experimental studies. Circ Res 1999;84:562–570.
[25] Hasenfuss G. Alterations of calcium-regulatory proteins in heart failure. Cardiovasc Res 1998;37:279–289.
[26] Chen X, Piacentino V, Furukawa S, Goldman B, Marguiles KB, Houser SR. L-type Ca^{2+} channel density and regulation are altered in failing human ventricular myocytes and recover after support with mechanical assist devices. Circ Res 2002;91:517–524.
[27] Schroder F, Handrock R, Beuckelmann DJ et al. Increased availability and open probability of single L-type calcium channels from failing compared with nonfailing human ventricle. Circulation 1998;98:969–976.
[28] Vatner DE, Sato N, Kiuchi K, Shannon RP, Vatner SF. Decrease in myocardial ryanodine receptors and altered excitation–contraction coupling early in the development of heart failure. Circulation 1994;90:1423–1430.
[29] Cory CR, Shen H, O'Brien PJ. Compensatory asymmetry in down-regulation and inhibition of the myocardial Ca^{2+} cycle in congestive heart failure produced in dogs by idiopathic dilated cardiomyopathy and rapid ventricular pacing. J Mol Cell Cardiol 1994;26:173–184.
[30] Pieske B, Maier LS, Bers DM, Hasenfuss G. Ca^{2+} handling and sarcoplasmic reticulum Ca^{2+} content in isolated failing and nonfailing human myocardium. Circ Res 1999;85:38–46.
[31] Dipla K, Mattiello JA, Margulies KB, Jeevanandam V, Houser SR. The sarcoplasmic reticulum and the Na^{+}/Ca^{2+} exchanger both contribute to the Ca^{2+} transient of failing human ventricular myocytes. Circ Res 1999;84:435–444.
[32] Hobai IA, O'Rourke B. Decreased sarcoplasmic reticulum calcium content is responsible for defective excitation–contraction coupling in canine heart failure. Circulation 2001;103:1577–1584.
[33] Haddock PS, Coetzee WA, Cho E et al. Subcellular $[Ca^{2+}]_i$ gradients during excitation-contraction coupling in newborn rabbit ventricular myocytes. Circ Res 1999;85:415–427.
[34] Litwin SE, Zhang D, Bridge JH. Dyssynchronous Ca(2+) sparks in myocytes from infarcted hearts. Circ Res 2000;87:1040–1047.